Budgeting and control of the mechanical noise in the International Linear Collider final focus system

D. Tshilumba,[1] M. Oriunno,[2] T. Markiewicz,[2] and C. Collette[1]

[1]*Université Libre de Bruxelles, BEAMS Department, 50 F.D. Roosevelt Avenue, 1050 Brussels, Belgium*
[2]*SLAC National Accelerator Laboratory, 2575 Sand Hill Road, Menlo Park, California 94025, USA*

(Received 26 December 2013; published 11 June 2014)

In this paper, we present a simplified vibration model of the silicon detector (SiD), where the final doublet (QD0) is captured inside the detector and the penultimate magnet (QF1) is inside the machine tunnel. Ground motion spectra measured at the detector hall at SLAC have been used together with a spectrum of the technical noise on the detector. The model predicts that the maximum level of rms (root mean square) vibration seen by QD0 is well below the capture range of the interaction point (IP) feedback system available in the ILC. With the addition of an active stabilization system on QD0, it is also possible to get closer to the stability requirements of the compact linear collider (CLIC). These results can have important implications for CLIC.

DOI: 10.1103/PhysRevSTAB.17.062801 PACS numbers: 45.80.+r, 46.40.Ff

I. INTRODUCTION

Ground motion and mechanical vibration can be major sources of luminosity loss at the final focus system (FFS) of future linear colliders, where the beams are nanometric and are required to be stable to better than a fraction of their size [1]. Reliable vibration models are therefore needed during the design process to establish the effectiveness of the supporting scheme to be adopted to protect the FFS from external vibration sources [2].

The beam structure of an ILC [3] bunch train (1312 bunches spaced by 554 ns) allows for an intratrain feedback system that measures the beam-beam deflection and drives a correction kicker. The sensitivity to jitter is thereby increased from the beam size (∼7 nm) to the capture range of the feedback system (∼1 um), which is set by the strength of the beam-beam deflection and the resolution of the beam position monitor (BPM) that measures the resulting displacement. The smaller the jitter is between bunch trains, the fewer number of bunches required to bring the beams into collision. The goal in the ILC has been to keep the incoming jitter to less than 200 nm, where the resultant luminosity loss is calculated to be less than 4% [4].

For the CLIC [5–7] beam structure intratrain feedback is less efficient and a combination of a careful design of the support structures with an active stabilization system is required [8–10], in combination with a repositioning system [11] and a preisolator [12]. The CLIC final doublet is required to be as stable as 0.15 nm above 4 Hz [5]. The requirement of maximizing the luminosity leads to optical schemes with the final doublet very close to the IP (∼4 m), captured in the innermost part of the forward region of the detector, which adversely affects the so-called "push-pull" operation mode where two detectors need to quickly (in a few days) swap their position on the IP after each (∼1 month long) data run. The silicon detector (SiD) detector [13] at the ILC has developed a support scheme

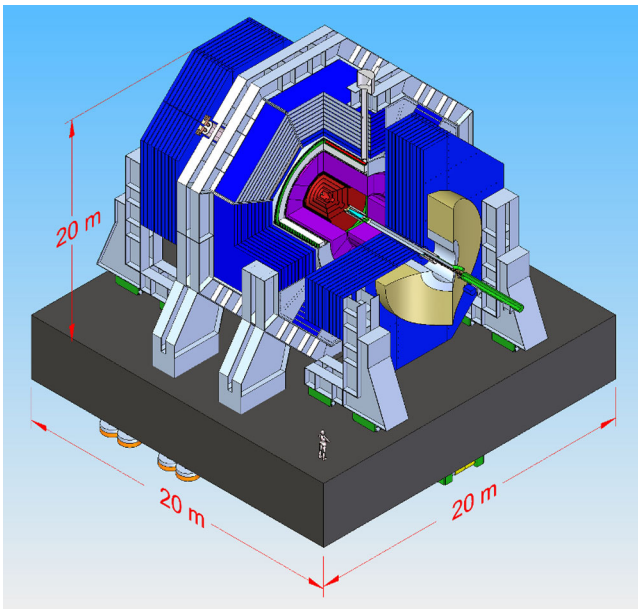

FIG. 1. Artist's view of the ILC SiD. The QF1 cryostat is pictured in green and is supported by the tunnel floor (which, for clarity, is not drawn). The QD0 cryostat is contained within the gray support tube visible in the cutaway of the iron door. These two magnet assemblies are connected by a ∼2 m piece of beampipe housing, on the input beam leg, the feedback system's stripline kicker (which appears in black).

for the FFS which allows both the reduction of the mechanical vibrations and a "fast" push-pull position exchange [14]. If coupled with an active stabilization system [15], this design can be applied effectively also to CLIC, where the IP feedback system is not as efficient. In the SiD scheme the QD0 quadrupole cryostat is supported directly on the iron of the flux return "door" and therefore moves with the detector, while the QF1 magnet cryostat is stationary in the machine tunnel (Fig. 1). In order to evaluate the level of vibration seen by the QD0 and the QF1 we developed in MATLAB a linear vibration model with lump mass and springs, which represent the fundamental parts of the detector. The state variables are the vertical degrees of freedom and the input variables are the ground vibrations and the detector noise generated by the technical systems on the detector. A closed loop analysis has been implemented to study the effects of the active stabilization. The paper is organized as follows. Section II presents the numerical model of the final focus, including the model of the beams, Sec. III presents the seismic response obtained with new measurements on site. Section IV studies the influence of two important parameters on the response, i.e. the stiffness of the ground and the amount of technical noise. Section V shows an objective figure of the benefit of quadrupole vibration isolation in a noisy environment, and Sec. VI draws the conclusions.

II. DESCRIPTION OF THE MODEL

A simplified model of the SiD detector is shown in Fig. 2. The last four quadrupoles (QD0 and QF1 on each side) are represented by masses m_0 and m_1. The detector structure, represented by m_s, is supported on a rigid platform, represented by m_p. Both have a vertical and tilt degree of freedom. The dominant mass of the detector is the iron for the flux return of the magnetic field. Although the iron is split in two doors and a central barrel, in working condition the mass of the doors is attracted by large forces toward the barrel, making a single lumped mass a good approximation of the dynamic behavior of the detector. That is also true for the platform, which is a single solid slab of reinforced concrete. The system includes also a model of the ground, represented by k_g [16].

The dynamics of the system reads

$$M\ddot{x} + C\dot{x} + Kx = Ew, \tag{1}$$

where

$$x = (x_1^+ x_1^- x_0^+ x_0^- x_s \theta_s x_p \theta_p)^T, w = (w_1^+ w_0^+ w_1^- w_0^-)^T, M = \mathrm{diag}(m_1 m_1 m_0 m_0 m_s I_s m_p I_p),$$

$$K = \begin{pmatrix} k'_q & 0 & 0 & 0 & 0 & 0 & 0 & 0 \\ 0 & k'_q & 0 & 0 & 0 & 0 & 0 & 0 \\ 0 & 0 & k_q & 0 & -k_q & Lk_q & 0 & 0 \\ 0 & 0 & 0 & k_q & -k_q & -Lk_q & 0 & 0 \\ 0 & 0 & -k_q & -k_q & 2(k_q + k_s) & 0 & -2k_s & 0 \\ 0 & 0 & Lk_q & -Lk_q & 0 & 2L^2(k_q + k_s) & 0 & -2L^2 k_s \\ 0 & 0 & 0 & 0 & -2k_s & 0 & 2(k_s + k'_p) & 0 \\ 0 & 0 & 0 & 0 & 0 & -2L^2 k_s & 0 & 2L^2(k_s + k'_p) \end{pmatrix},$$

$$C = \begin{pmatrix} c'_q & 0 & 0 & 0 & 0 & 0 & 0 & 0 \\ 0 & c'_q & 0 & 0 & 0 & 0 & 0 & 0 \\ 0 & 0 & c_q & 0 & -c_q & Lc_q & 0 & 0 \\ 0 & 0 & 0 & c_q & -c_q & -Lc_q & 0 & 0 \\ 0 & 0 & -c_q & -c_q & 2(c_q + c_s) & 0 & -2c_s & 0 \\ 0 & 0 & Lc_q & -Lc_q & 0 & 2L^2(c_q + c_s) & 0 & -2L^2 c_s \\ 0 & 0 & 0 & 0 & -2c_s & 0 & 2(c_s + c'_p) & 0 \\ 0 & 0 & 0 & 0 & 0 & -2L^2 c_s & 0 & 2L^2(c_s + k'_p) \end{pmatrix},$$

$$E = \begin{pmatrix} k'_q + sc'_q & 0 & 0 & 0 \\ 0 & 0 & 0 & k'_q + sc'_q \\ 0 & 0 & 0 & 0 \\ 0 & 0 & 0 & 0 \\ 0 & 0 & 0 & 0 \\ 0 & 0 & 0 & 0 \\ 0 & k'_p + sc'_p & k'_p + sc'_p & 0 \\ 0 & -L(k'_p + sc'_p) & L(k'_p + sc'_p) & 0 \end{pmatrix}, \quad k'_p = \frac{k_p k_g}{k_p + k_g}; \qquad c'_p = \frac{c_p c_g}{c_p + c_g};$$

$$k'_q = \frac{k_q k_g}{k_q + k_g}; \qquad c'_q = \frac{c_q c_g}{c_q + c_g}.$$

Dashpots are added in parallel with each spring, using the same subscripts as the stiffness. They are not shown for the clarity of Fig. 2 but are taken into account in all of the calculations. M is the mass matrix, C is the damping matrix, K is the stiffness matrix, w is the vector of ground motion, and E is the matrix of excitations.

The parameter values listed in Table I were calculated as follows: mass and inertia properties have been calculated by design software. The stiffness parameters were estimated with a simplified finite element model of the single parts. Based on our experience, we have assumed a damping ratio of 5%, which is a typical value for such a structure. This assumption led to the coefficients mentioned in Table I. The values of L_0 and L_1, along with the detailed baseline design of the SiD can be found in [17].

From the dynamic equation above, we can calculate the matrix of the transfer function as

$$\boldsymbol{H}(s) = (\boldsymbol{M}s^2 + \boldsymbol{C}s + \boldsymbol{K})^{-1}\boldsymbol{E},$$

where s is the Laplace variable. The magnitudes of the transfer functions from the ground to the quadrupoles are shown in Fig. 3. We see on the figure that the quality factor of the four peaks below 30 Hz is about 10, i.e. that the modal damping is around 5%.

In the model described in Fig. 2, the beam-beam offset at the interaction point y, in the thin lens approximation, is

$$y = C_0(x_0^+ - x_0^-) + C_1(x_1^+ - x_1^-),$$

where C_0 is the transport matrix element from QD0 to the IP, $C_0 = \mathrm{K(QD0)} * \mathrm{Length(QD0)} * \mathrm{DL(QD0 - IP)}$ and where C_1 is the transport matrix element from QF1 to QD0 times that from QD0 to the IP,

$$C_1 = C_0 * \mathrm{K(QF1)} * \mathrm{Length(QF1)} * \mathrm{DL(QF1 - QD0)}.$$

Here K(QF1) and K(QD0) are the beam-momentum normalized curvatures in $1/\mathrm{m}^2$ from the optics decks. Using the notation described above, y can be expressed as

$$y = Rx,$$

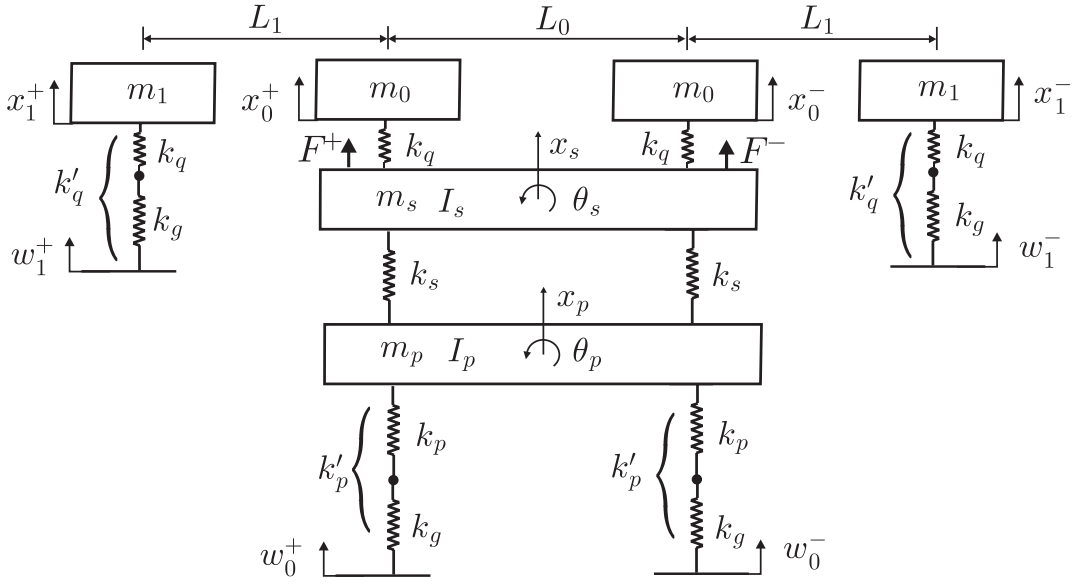

FIG. 2. Lumped mass model of the ILC final focus with the SiD configuration.

TABLE I. Numerical values of the parameters.

Variable	Value	Units
m_1	1,00E + 03	(Kg)
m_0	1,00E + 03	(Kg)
m_s	8,00E + 06	(Kg)
m_p	3,49E + 06	(Kg)
I_s	1,34E + 08	(Kg m^2)
I_p	1,21E + 08	(Kg m^2)
k_q	1,00E + 09	(N/m)
k_g	1,00E + 11	(N/m)
k_p	3,48E + 10	(N/m)
k_s	3,16E + 10	(N/m)
c_q	1,41E + 05	(Ns/m)
c_g	5E + 06	(Ns/m)
c_p	1,15E + 07	(Ns/m)
c_s	6,28E + 04	(Ns/m)
L_0	10	(m)
L_1	6	(m)
L	5	(m)

where $R = [C_1 - C_1C_0 - C_00000]$, $C_0 = 1.27$, and $C_1 = -0.466$ [18].

III. SEISMIC RESPONSE

From (1), we can calculate the matrix of power spectral densities as

$$S_x(\omega) = HS_w(\omega)H^*,$$

where * represents the conjugate transposed operator and ω is the angular frequency. The power spectral density of the beam-beam offset is given by [19]

$$S_y(\omega) = (RH)S_w(\omega)(RH)^*.$$

The matrix of excitations $S_w(\omega)$ is given by

$$S_w(\omega) = \begin{pmatrix} \Phi_{w_1^+} & \Phi_{w_1^+w_0^+} & \Phi_{w_1^+w_0^-} & \Phi_{w_1^+w_1^-} \\ \cdots & \Phi_{w_0^+} & \Phi_{w_0^+w_0^-} & \Phi_{w_0^+w_1^-} \\ \cdots & \cdots & \Phi_{w_0^-} & \Phi_{w_0^-w_1^-} \\ SYM & \cdots & \cdots & \Phi_{w_1^-} \end{pmatrix},$$

where Φ is the power spectral density (PSD) of the quantity in subscript [if two quantities appear in the subscript, it represents the cross PSD (CPSD) between the two quantities]. From Φ, the integrated (downwards) root mean square (rms) value, noted $\sigma(\omega)$, is defined as

$$\sigma(\omega) = \sqrt{\int_{\omega}^{+\infty} \Phi(\omega) d\omega}.$$

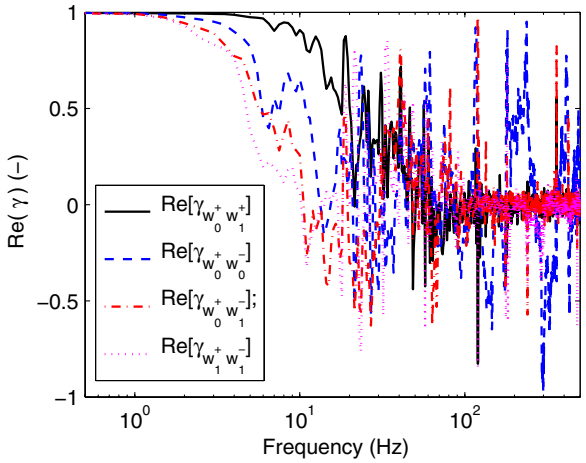

FIG. 4. Real part of the correlation between the ground motions at the support locations.

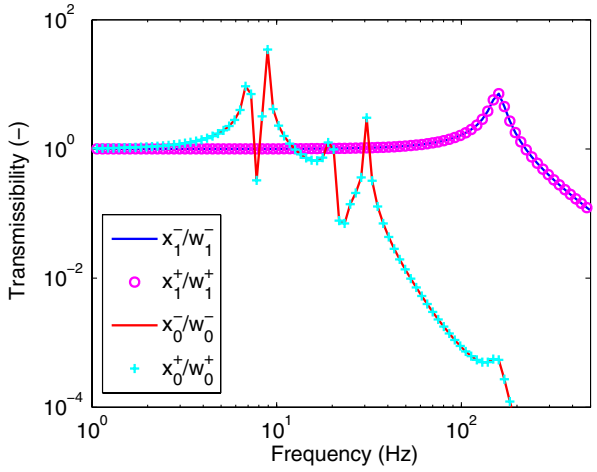

FIG. 3. Transfer functions between the ground and the quadrupoles.

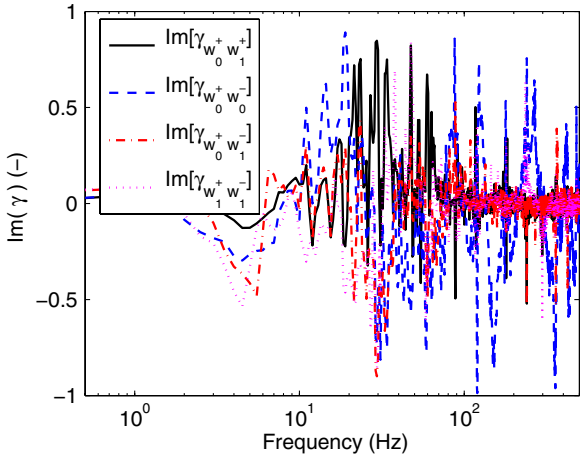

FIG. 5. Imaginary part of the correlation between the ground motions at the support locations.

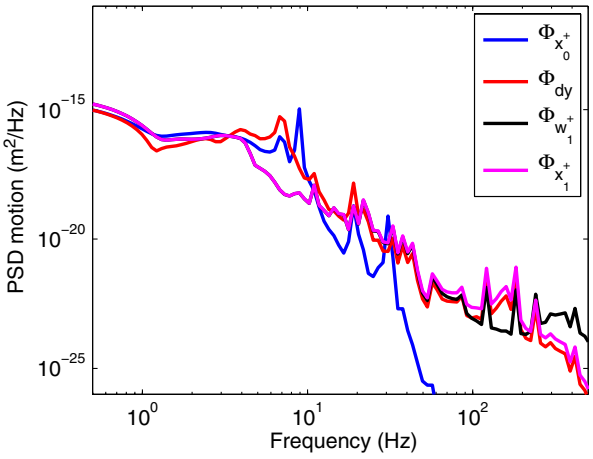

FIG. 6. Power spectral densities of the seismic response, without technical noise.

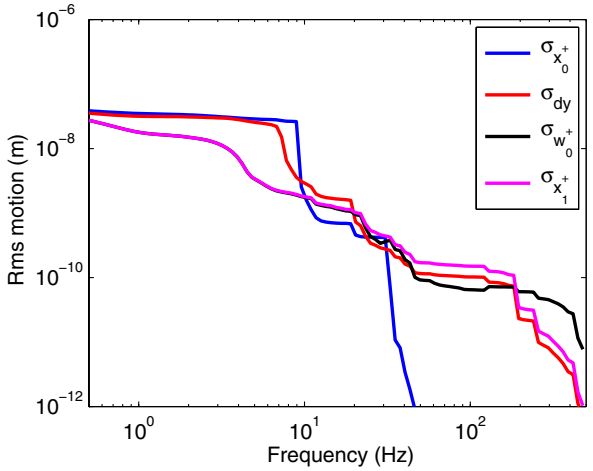

FIG. 7. Integrated rms without technical noise.

The ground motion spectra which have been used for the simulations were measured at the SLAC Large Detector (SLD) hall. As the system is symmetrical, we will assume $\Phi_{w_1^+} = \Phi_{w_1^-}$; $\Phi_{w_0^+} = \Phi_{w_0^-}$; $\Phi_{w_1^+ w_0^+} = \Phi_{w_0^- w_1^-}$; $\Phi_{w_1^+ w_0^-} = \Phi_{w_0^+ w_1^-}$; $\Phi_{w_1^+ w_0^-} = \Phi_{w_1^+ w_1^-}$; $\Phi_{w_1^+ w_0^-} = \Phi_{w_1^+ w_0^+}$. The real and imaginary parts of the normalized spectral densities are shown in Figs. 4 and 5 [20].

It has been found that the new measurements correlate well with previous campaigns (see [21] and the references therein). Figure 6 shows the power spectral densities of the quadrupoles displacements ($\Phi_{x_0^+}$, $\Phi_{x_1^+}$) and the beam-beam offset (Φ_{dy}). Figure 7 shows the corresponding integrated rms values.

IV. PARAMETER VARIATION

In addition to any fast intratrain feedback, all linear colliders incorporate a "slow" feedback system to control vibration or drift at lower frequencies. The machine bunch train repetition frequency, 5 Hz for the ILC, sets the scale at which the slow feedback system can correct potentially larger drifts. For the ILC, in order to keep the luminosity loss to less than 4%, the jitter between the bunch trains, σ_y, should not exceed 200 nm [4]. For this reason, we will study the effect of two important parameters (the ground stiffness and the technical noise) on σ_y at 5 Hz.

A. Effect of the ground stiffness

The ground stiffness k_g is a parameter of significant importance. The lower the ground stiffness value is, the more relevant the role of the QF1 doublet is in the beam-beam jitter at the interaction point.

When the k_g parmeter value is low (e.g. $k_g = 3e8N/m$), the first peaks of resonance of the QD0 transmissibility are shifted to the left, which leads to substantial isolation at 5 Hz. In that scenario, the limiting factor for the luminosity quality is the stability of the QF1 doublet. Alternatively when the ground stiffness is high (e.g. $k_g = 1e11N/m$), the resonance frequency of QD0 is larger, which compromises

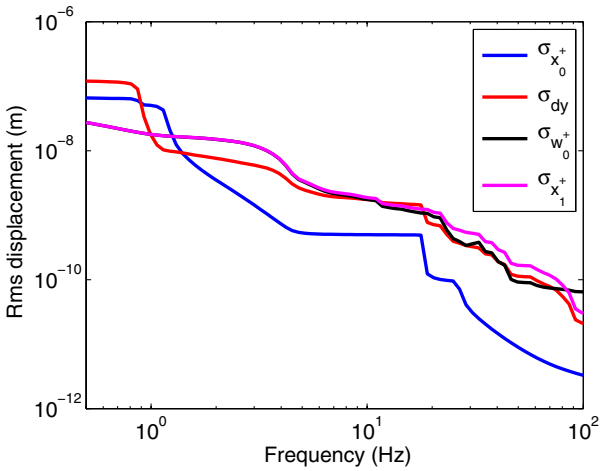

FIG. 8. Integrated rms for $k_g = 3e8N/m$.

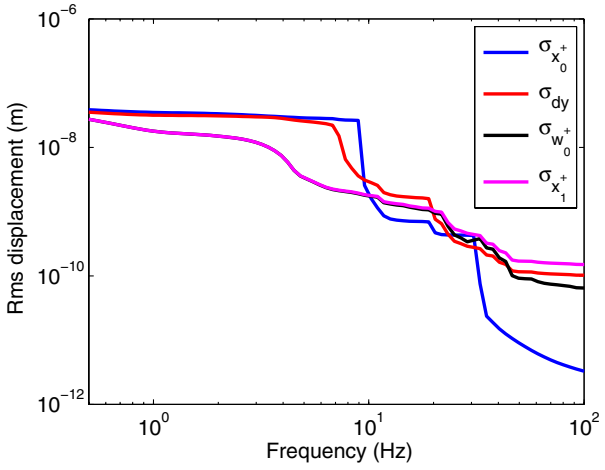

FIG. 9. Integrated rms for $k_g = 1e11N/m$.

the isolation. In that scenario, the beam-beam jitter is mainly determined by the QD0 doublet stability. Figures 8 and 9 show a comparison of both scenarios.

B. Effect of the technical noise

The technical noise includes various types of incoherent environmental disturbances (electronics, ventilation, cooling, etc.). In this study, it is represented by random forces. Even though cross-correlation may exist between these forces, we prefer to adopt a conservative approach and neglect all cross-correlations. Two models have been considered.

In the first one, used to model the disturbances applied on the detector mass m_s (F^+ and F^- in Fig. 2), the PSD of the force is decreasing at low frequency as

$$\Phi_{F^+} = \Phi_{F^-} = \frac{N_0 f^2}{1 + (\frac{f}{f_0})^4},$$

where f is the frequency and N_0 and f_0 are parameters. N_0 is the amplitude of the noise and f_0 is the corner frequency [18]. It is assumed that F^+ and F^- are not correlated, i.e. that their cross PSD is equal to zero. We take $N_0 = 10^{-2}(N^2/Hz^3)$ and $f_0 = 21(Hz)$. Using these values, the rms value integrated over the whole frequency range is $\sigma_{F^+} = \sigma_{F^-} = 10(N)$, which is a reasonable assumption, based on our personal experience and previous measurement campaigns [19,20].

The second model is used to model the disturbances applied directly on the quadrupoles. The PSD of the typical white noise describing vibrations coming from water cooling, ventilation, and acoustic noise is given by

$$\Phi_{F_2} = \frac{N_{02}}{1 + (\frac{f}{f_{02}})^2},$$

where f is the frequency, $N_{02} = 0.75(\frac{N^2}{Hz})$, and $f_{02} = 35(Hz)$. N_{02} is the amplitude, and f_{02} is the phase. Both models are shown in Fig. 10.

In order to evaluate the acceptable level of technical noise, we have calculated the beam-beam offset for various amplitudes of the disturbing force, ranging from $N_{02} = 0.75(\frac{N^2}{Hz})$ to $N_{02} = 2.5(\frac{N^2}{Hz})$ (i.e. a variation of the rms value from $\sigma_{F2,\min} = 0.02N$ to $\sigma_{F2,\max} = 11N$). The same comment holds for the choice of the value of N_{02} and f_{02} as for the choice of N_0 and f_0.

Figure 11 shows a quadratic evolution of σ_y at 5 Hz as a function of the amplitude of the technical noise σ_{F2} applied on the QD0 doublet, which is cooled by superfluid helium II. The maximum expected amplitude range for helium II is ~10 N rms and the corresponding σ_y is 50 nm, well below the 200 nm capture range of the IP feedback system.

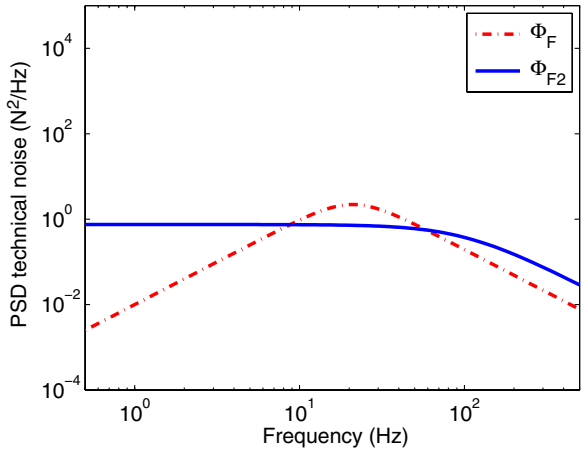

FIG. 10. Power spectral densities of the two technical noise assumptions. Φ_F is the technical noise applied on the detector and Φ_{F2} is the technical noise applied on QD0.

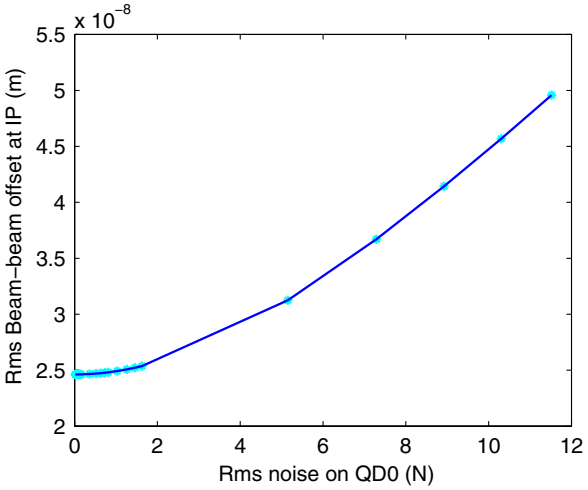

FIG. 11. Evolution of the beam-beam offset at the interaction point σ_y at 5 Hz as a function of the amplitude of the technical noise on QD0.

V. DOUBLETS VIBRATION ISOLATION

A. Passive isolation

In order to investigate the effect of the isolation of the QF1s on σ_{x_1} and σ_y, we consider a small value of F_2, i.e. $\sigma_{F2,\min} = 0.02N$. Then, we decrease resonance frequency f_{QF1} of the QF1 by decreasing the stiffness below QF1. As f_{QF1} decreases, the passive isolation of the QF1 increases, and at some point both the QD0 and the QF1 contribute to σ_y by the same amount.

The results of the simulations for which $f_{QF1} = 2$ Hz, $f_{QF1} = 7$ Hz, and $f_{QF1} = 150$ Hz are shown in Figs. 12, 13, and 14, respectively.

Figure 15 shows the evolution of the rms value of the beam-beam offset integrated down to 5 Hz, $\sigma_{y,5\,\mathrm{Hz}}$, as a function of the resonance frequency of QF1 on its support stiffness.

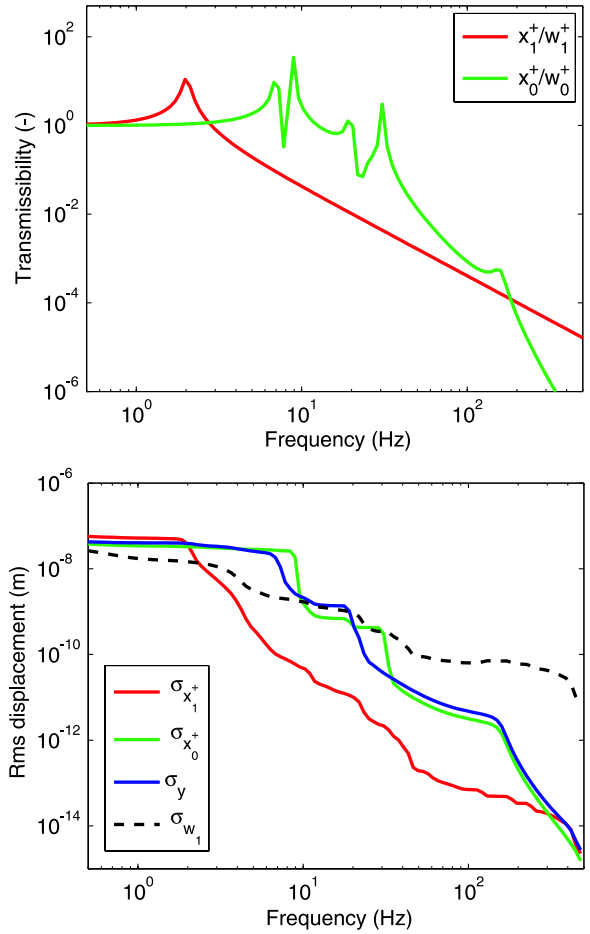

FIG. 12. Transfer functions and integrated rms values of the quadrupoles response for $f_{\mathrm{QF1}} = 2Hz$ with $\sigma_{\mathrm{F2}} = 0.02N$.

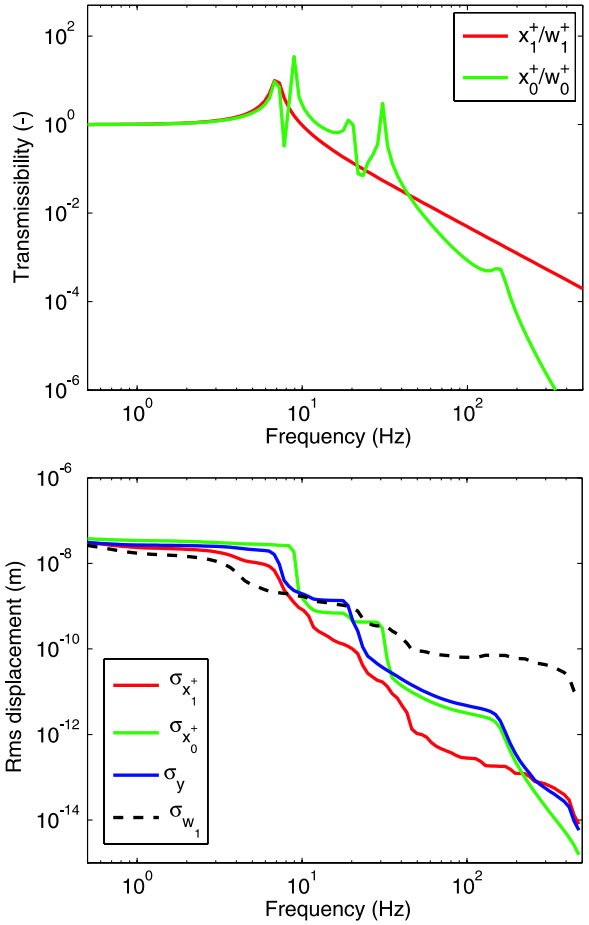

FIG. 13. Transfer functions and integrated rms values of the quadrupoles response for $f_{\mathrm{QF1}} = 7Hz$ with $\sigma_{\mathrm{F2}} = 0.02N$.

For high values of f_{QF1} (i.e $f_{\mathrm{QF1}} \geq 20$ Hz), the stiffness k'_q is so significant that the response σ_{x1} follows exactly the excitation σ_{w1} at low frequency. In that case σ_{x1} is one order of magnitude smaller than σ_{x0} at 5 Hz. Therefore the beam-beam offset at 5 Hz is essentially independent of f_{QF1} (the curve in Fig. 15 is flat above 20 Hz).

For low values of f_{QF1} (i.e $f_{\mathrm{QF1}} \leq 3$ Hz), the stiffness k'_q is so low that some isolation with regard to σ_{w1} is already introduced to the response σ_{x1} of the QF1 at 5 Hz. As a result σ_{x1} is at least 2 orders of magnitude smaller than σ_{x0} at 5 Hz. Consequently the beam-beam offset at 5 Hz is independent of f_{QF1} (the curve in Fig. 15 is flat below 3 Hz).

For intermediate values of f_{QF1} (i.e. 3 Hz $\leq f_{\mathrm{QF1}} \leq$ 20 Hz), σ_{x1} and σ_{x0} have the same order of magnitude at 5 Hz. In that case the beam-beam offset at 5 Hz is sensitive to the isolation of the QF1.

B. Active isolation

In this section, we study the capability of an active isolation of the quadrupoles on the beam-beam offset. The strategy chosen for the active isolation is based on inertial feedback, where the absolute displacement of each quadrupole is measured with an inertial sensor, filtered by a controller, and fed back in individual actuators located in parallel with each spring of stiffness k_q. All inertial sensors are assumed identical: they are made up of one d.o.f. oscillator, with a typical resonance of 2 Hz, and the percentage of damping is 0.3 [22]. These values are typical of commercial geophones. In order to achieve the best compromise between isolation from ground vibrations and robustness to external disturbances (the technical noise), we start with an intermediate configuration where the resonance frequencies of the quadrupoles have been decreased at 15 Hz. For this, the stiffness value of the link between QF1 and the ground has been modified to $k_q = 1e7N/m$. This configuration corresponds typically to a big mass placed on a rubber layer in series with a piezoelectric actuator [23]. Figure 16 shows the transfer functions between the ground and the quadrupoles when the feedback control is turned off and on. The same controller is applied to the four feedback loops: a lag at low frequency and a lead at high frequency. This controller is written

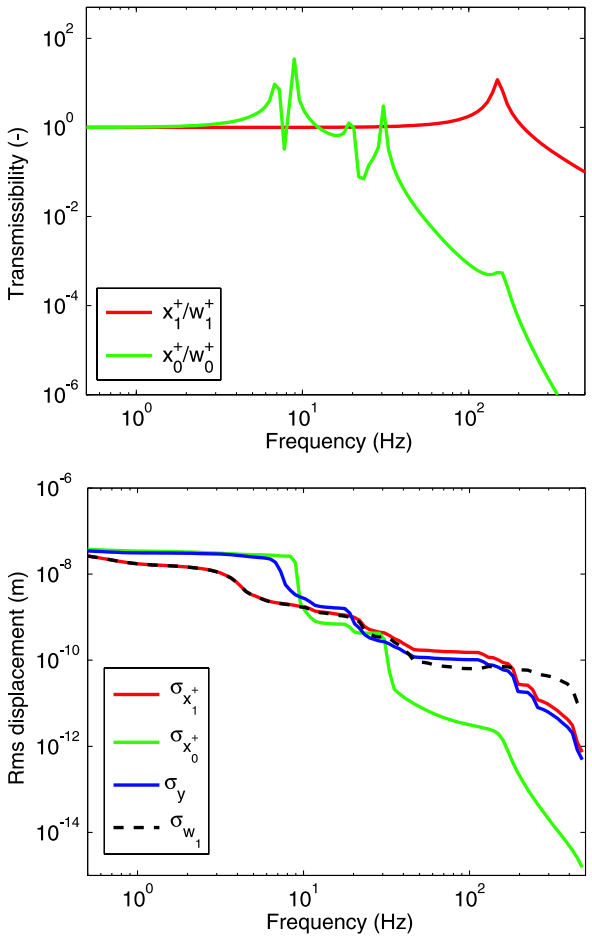

FIG. 14. Transfer functions and integrated rms values of the quadrupoles response for $f_{\mathrm{QF1}} = 150Hz$ with $\sigma_{\mathrm{F2}} = 0.02N$.

$$C(s) = 10^{10} \times \frac{3.356\ \mathrm{s}^2 + 5.858\mathrm{e}2\ \mathrm{s} + 3.895\mathrm{e}3}{\mathrm{s}^2 + 2.621\mathrm{e}4\ \mathrm{s} + 1.317\mathrm{e}4}.$$

This filter is used to increase the phase margins at the crossover frequencies. An interesting advantage of this active isolation strategy is that it increases the isolation at low frequency, and also improves the robustness to the technical noise, which is only possible with an active system. Figure 17 shows the response (integrated rms) when the controller is turned on and when it is turned off. As the technical noise $\sigma_{F2} = 10N$ rms which is applied is the dominant perturbation on QD0, the contribution of the ground vibrations to the rms displacement σ_{x0} is negligible. The results shown in Fig. 17 indicate that, in principle, a very good level of stability can be reached, at least provided that the noise floor of the hardware (sensor, controller, and actuator) is sufficiently low to avoid the reinjection of noise. In particular, the stability level of QD0 is well below the requirements of the ILC but not good enough for those of CLIC. However, the active control strategy enables the QF1 to reach the stability requirements of CLIC.

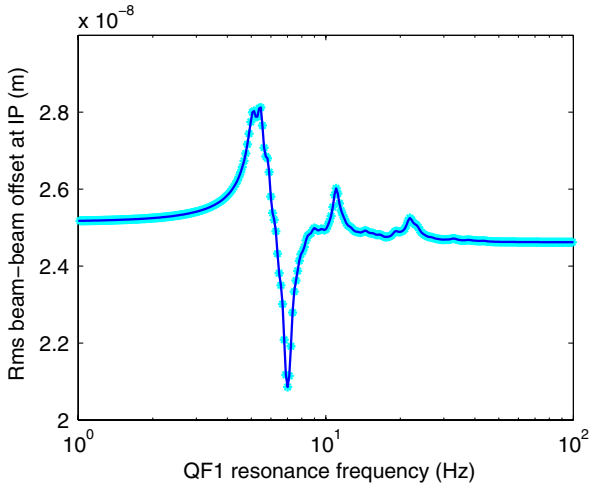

FIG. 15. Beam-beam offset integrated down to 5 Hz as a function of the resonance frequency of the QF1s.

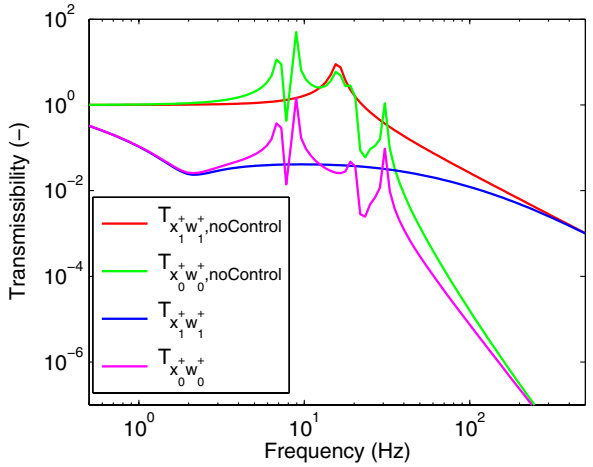

FIG. 16. Transfer functions between the ground and the quadrupoles, with and without control.

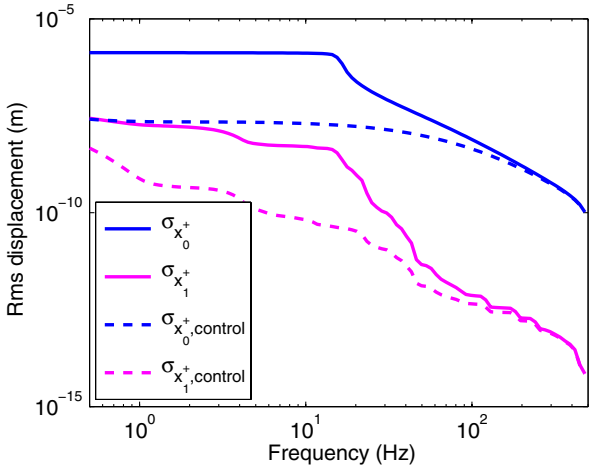

FIG. 17. Integrated rms when the control is turned on and off.

VI. CONCLUSION

We developed a simplified vibration model of the SiD detector, where the QD0 doublet is captured inside the detector and the QF1 magnet is inside the machine tunnel. Ground motion spectra measured at the SLD detector hall at SLAC have been used together with a conservative spectrum of the technical noise on the detector. The objective is to identify the important parameters, and make an assessment of their impact on the beam jitter at the IP, especially in the presence of technical noise. It has been found that the stiffness of the ground, the level of technical noise, and the dynamics of the QF1s play a significant role. Using the chosen set of parameters, the model predicts that the maximum level of rms vibration seen by QD0 is well below the target value for 4% luminosity loss of the IP feedback system available in the ILC. However this level of vibration is still too high for CLIC. With the addition of an active stabilization system, it has been shown that it is possible for QF1 to reach the stability requirements of CLIC. These preliminary conclusions need to be confirmed by a more realistic finite element model of the SiD, including more complex geometries, inertia, and flexibilities. The models of the technical noise need also to be correlated with experimental measurements, which are planned in the near future.

ACKNOWLEDGMENTS

This research has been funded by the Brussels capital region under the program "Brains back to Brussels." The authors also gratefully acknowledge Paul Marty for his help with the numerical simulations. The comments of the reviewers have significantly contributed to improve the quality of the manuscript.

[1] A. Seryi, M. Breidenbach, and J. Frisch, in *Proceedings of the 20th International Linac Conference, LINAC-2000, Monterey, CA* (SLAC, Menlo Park, CA, 2000).

[2] A. Seryi, Nucl. Instrum. Methods Phys. Res., Sect. A **623**, 23 (2010).

[3] The ILC TDR, Vol. **4** (Detectors), Sec. 7.4.5, 2013 [http://www.linearcollider.org/ILC/Publications/Technical-Design-Report].

[4] P. N. Burrows, D. R. Bett, N. Blaskovic Kraljevic, G. B. Christian, M. R. Davis, Y. I. Kim, C. Perry, R. J. Apsimon, B. Constance, and A. Gerbershagen, *Proceedings of the 4th International Particle Accelerator Conference, IPAC-2013, Shanghai, China, 2013* (JACoW, Shanghai, China, 2013).

[5] CLIC Conceptual Design Report, CERN-2012-007, Geneva, Switzerland, 2012.

[6] J. P. Delahaye, in *Proceedings of the International Particle Accelerator Conference, Kyoto, Japan* (ICR, Kyoto, 2010).

[7] F. Simon, Phys. Procedia **37**, 63 (2012).

[8] C. Collette, D. Tshilumba, L. Fueyo-Rosa, and I. Romanescu, Rev. Sci. Instrum. **84**, 023302 (2013).

[9] C. Collette, S. Janssens, and D. Tshilumba, Nucl. Instrum. Methods Phys. Res., Sect. A **684**, 7 (2012).

[10] R. Le Breton, G. Deleglise, J. Allibe, A. Badel, G. Balik, B. Caron, and A. Jeremie, Sens. Actuators A **204**, 97 (2013).

[11] F. Lackner, K. Artoos, C. Collette, H. Mainaud Durand, C. Hauviller, J. Kemppinen, and R. Leuxe, *Proceedings of the 6th International Workshop on Mechanical Engineering Design of Synchrotron Radiation Equipment and Instrumentation (MEDSI00), Oxford, United Kingdom, 2010* (Cambridge University Press, Cambridge, England, 2011).

[12] A. Gaddi, H. Gerwig, N. Siegrist, and F. Ramos, Technical Report EDMS n1098581, 2010.

[13] H. Aihara *et al.*, arXiv:0911.0006.

[14] B. Parker, A. Mikhailichenko, K. Buesser, J. Hauptman, T. Tauchi, P. Burrows, T. Markiewicz, M. Oriunno, and A. Seryi, Technical Report EuCARD-CON-2009-026, 2009.

[15] J. Frisch, A. Chang, V. Decker, E. Doyle, L. Eriksson, L. Hendrickson, T. Himel, T. Markiewicz, R. Partidge, and A. Seryi, *Proceedings of the 22nd International Linear Collider Conference, LINAC-2004, Lübeck, Germany, 2004* [http://accelconf.web.cern.ch/accelconf/l04/PAPERS/THP35.PDF].

[16] K. Bertsche, J. W. Amann, T. W. Markiewicz, M. Oriunno, A. Weidemann, and G. White, *Proceedings of the 3rd International Particle Accelerator Conference, IPAC-2012, New Orleans, LA* (IEEE, Piscataway, NJ, 2012), TUPPR047; , Report No. SLAC-PUB-15027, 2012.

[17] T. Behnke, J. Brau, P. Burrows, J. Fuster, M. Peskin, M. Stanitzki, Y. Sugimoto, S. Yamada, and H. Yamamoto, International Linear Collider Technical Design Report, Vol. **4**, No. ILC-REPORT-040, 2013.

[18] Glen White, SLAC (private communication).

[19] C. Collette, K. Artoos, M. Guinchard, and C. Hauviller, Phys. Rev. ST Accel. Beams **13**, 072801 (2010).

[20] K. Bertsche and A. Weidemann, "Geophone Measurements on SLD," SiD MDI Meeting, 2010.

[21] A. Sery, and O. Napoly, Phys. Rev. E **53**, 5323 (1996).

[22] C. Collette, P. Fernandez-Carmona, S. Janssens, K. Artoos, M. Guinchard, C. Hauviller, and A. Preumont, *BSSA,**102**, 1289 (2012).*

[23] C. Collette, S. Janssens, K. Artoos, *Recent Patents on Mechanical Engineering **4**, 212 (2011)* [http://www.ingentaconnect.com/content/ben/meng/2011/00000004/00000003/art00002;jsessionid=deoslq9h0bmm8.alice.